

## Demonstration of aluminum $K$ -shell line shifts in isochorically heated targets driven by ultrashort laser pulses

U. ANDIEL<sup>1</sup>, K. EIDMANN<sup>1</sup>, P. HAKEL<sup>2</sup>, R. C. MANCINI<sup>2</sup>,  
G. C. JUNKEL-VIVES<sup>3†</sup>, J. ABDALLAH<sup>3</sup> and K. WITTE<sup>1</sup>

<sup>1</sup> *Max-Planck-Institut für Quantenoptik - D-85748 Garching, Germany*

<sup>2</sup> *Department of Physics, University of Nevada - Reno, NV 89557-0058, USA*

<sup>3</sup> *Los Alamos National Laboratory - Los Alamos, NM 87545, USA*

(received 11 July 2002; accepted 27 September 2002)

PACS. 52.50.Jm – Plasma production and heating by laser beams (laser-foil, laser-cluster, etc.).

PACS. 32.30.Rj – X-ray spectra.

PACS. 32.70.Jz – Line shapes, widths, and shifts.

**Abstract.** – Targets consisting of 25 nm Al layers buried in solid carbon at depths of up to 400 nm have been irradiated with frequency doubled Ti:sapphire laser pulses of 150 fs duration at an intensity of a few  $10^{17}$  W/cm<sup>2</sup>. The analysis of the emitted Al  $K$ -shell spectra yields densities close to that of solid Al and temperatures around 500 eV. By using the cold Si  $K_{\alpha}$  line for wavelength calibration, the presence of a red dense-plasma line shift for several  $K$ -shell resonance and associated satellite lines is clearly demonstrated.

*Introduction.* – In hot dense strongly coupled plasma the orbitals of the radiating atoms are heavily perturbed by the presence of free plasma electrons. As a consequence, the emitted lines are broadened and undergo a red-shift [1], called in the following DPLS (dense-plasma line shift). Besides the basic interest in this phenomenon, the line emission from dense plasma is of practical relevance for the diagnostics of dense plasma, such as the plasma in the compressed core in inertial-confinement fusion (ICF) [2].

Based on quantum theory, the DPLS has been predicted by several authors [3–5]. It increases linearly with the electron density  $n_e$ , but remains small even at the largest densities of  $n_e \approx 10^{24}$  cm<sup>-3</sup> achieved in the laboratory. It is, therefore, not easy to demonstrate such small line shifts experimentally. The difficulties are caused by the presence of opacity effects and spatial inhomogeneities. Also, an independent calibration of the wavelength is critical. Evidence for a DPLS of the higher Rydberg members of  $K$ -shell lines emitted from C and Al plasmas generated with nanosecond laser pulses with  $n_e$  not larger than a few times  $10^{22}$  cm<sup>-3</sup> were obtained in [6, 7]. For even larger  $n_e$  ( $\approx 10^{24}$  cm<sup>-3</sup>), a red DPLS in the Ar He $_{\beta}$  line was found in an ICF plasma where Ar was used as a tracer gas [8]. Recently, it was demonstrated that comparable high densities can be obtained with high-intensity sub-picosecond laser pulses using much smaller laser installations compared to those needed for

---

† We regret to inform that G. C. Junkel-Vives passed away in December 2001.

ICF. By isochorically heating solid Al with 150 fs pulses, evidence for a DPLS of the Al Ly $_{\alpha}$  line and its He-like satellite and of the He $_{\beta}$  line has been previously observed [9].

In this letter we present a new experiment that clearly demonstrates the presence of DPLSs and is well suited to rigorously prove the theory. For this purpose, an ultrashort laser pulse irradiates a target consisting of a thin Al sample layer (SL) buried in solid carbon. The possibility of heating buried SLs up to temperatures of several 100 eV has already been shown in previous experiments [10–13]. For quantitative spectroscopy, this technique offers substantial advantages compared to our previous work [9] performed with massive Al targets. The small thickness of the SL results in a quasi-uniform plasma region. Also, opacity effects are less important, since the SL is thin. Embedding the SL at different depths results in different time-averaged densities, because a SL located deep inside the carbon will undergo slower expansion and result in higher densities compared to a SL placed close to the target surface. Thus, the DPLS can be studied systematically at different densities. Furthermore, the uniform plasma conditions in the SL simplify the theoretical interpretation and analysis of the spectra. This has been done by post-processing hydrodynamic temperature and density time histories with a transient collisional-radiative atomic kinetics model, and then using the level populations and detailed line shapes to produce synthetic spectra including and not including the effect of line shifts. In this way, deviations from the local thermal equilibrium (LTE) occurring in the strongly transient plasma are taken into account.

*Experiment.* – For target irradiation, we used a frequency doubled Ti:sapphire laser. It delivers an energy of  $\approx 60$  mJ in 150 fs pulses at  $\lambda = 395$  nm with a contrast ratio better than  $1 : 10^{10}$  in the temporal window 2–30 ns before the main pulse and better than  $1 : 10^6$  at 1 ps before the pulse maximum. The laser was focused by an off-axis parabolic mirror on the target yielding a spot of  $9 \mu\text{m}$  diameter for 80% of the incident energy. For the chosen angle of incidence of  $45^\circ$  and  $p$ -polarization, the absorption is typically 50% [14]. The layered target consisted of a massive plane substrate (made of Sigradur, a glass-like carbon modification), on which a 25 nm thick Al layer and a carbon tamper layer of variable thickness,  $d_c$ , in the range 25 nm to 400 nm were evaporated (see the inset of fig. 1). The Al  $K$ -shell emission was mea-

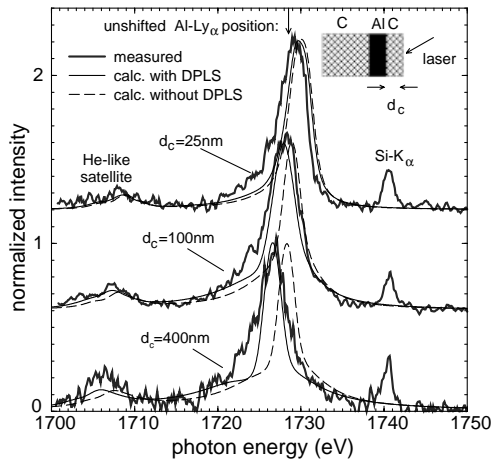


Fig. 1 – The Ly $_{\alpha}$  line with the Si  $K_{\alpha}$  reference line. The vertical arrow indicates the isolated atom unshifted Ly $_{\alpha}$  position, calculated by weighting statistically the two fine-structure components  $P_{1/2}$  and  $P_{3/2}$ . Spectra are vertically shifted for clarity.

sured by a conventional von Hamos spectrometer with a PET (pentaerythritol) crystal and an X-ray film as the detector. The spectral window ranged from the Al  $K_\alpha$  to the Al  $Ly_\beta$  at a spectral resolution of 0.9 eV. In each spectrum, typically 100 shots were accumulated at 10 Hz, with the laser always focused on a fresh spot of a rotating target. The typical size of the Al  $K$ -shell-emitting spot was about  $13\ \mu\text{m}$  (for 80% of the X-ray energy) as was measured by a penumbral technique. This results in a laser intensity of  $\approx 2.5 \times 10^{17}\ \text{W}/\text{cm}^2$ . In addition to the Al  $K$ -shell emission, we measured the bremsstrahlung in the region 5 to 40 keV yielding a typical hot-electron temperature of 9 keV. For further experimental details we refer the reader to ref. [15].

A fiducial wavelength is indispensable for an accurate determination of the wavelength axis. To this end, we used the cold Si  $K_\alpha$  line, which lies very close to the Al  $Ly_\alpha$  line and is therefore an excellent candidate to determine nearby line positions. Spectra with the Si  $K_\alpha$  reference line were generated by firing first on the Al SL target and then on a glass ( $\text{SiO}_2$ ) target. In order to enhance the intensity of the Si  $K_\alpha$  line, a prepulse was added to the main-pulse. Both spectra were superimposed on the same film. In our experiment, this procedure required only changing targets, while the spectrometer remained in the same position. In addition, the source remained within the target alignment accuracy of  $\pm 15\ \mu\text{m}$  at the same position. Thus, we are sure that the line positions on the film did not change by more than 0.05 eV, which is negligible compared to our spectral resolution of 0.9 eV. Figure 1 shows an example of the Al  $Ly_\alpha$  line at three different thicknesses  $d_c$  of the carbon tamper layer together with the superimposed Si  $K_\alpha$  reference line. The Si  $K_\alpha$  line is quite narrow (full width at half-maximum (FWHM) = 1.5 eV) and allows us to fix the  $h\nu$  scale in the vicinity of the Al  $Ly_\alpha$  line with an accuracy of  $\pm 0.3$  eV. The measured width is in agreement with the line shape of the  $K_\alpha$  line folded with our resolution of 0.9 eV (we note that the  $K_\alpha$  has the two components  $K_{\alpha 1}$  and  $K_{\alpha 2}$ , which are separated by 0.5 eV). In fig. 1 we clearly observe a systematic center-of-mass shift (CM shift) of a few eV of the Al  $Ly_\alpha$  line to lower energies with increasing  $d_c$ .

Measured Al spectra in the full spectral window are displayed in fig. 2 for three different thicknesses  $d_c$ . The absolute value given there is obtained from the film sensitivity and the

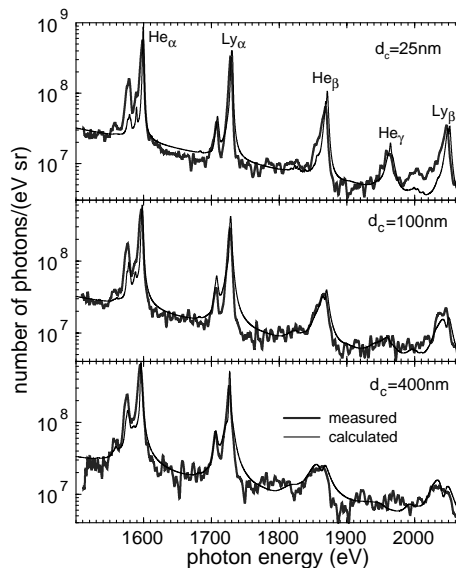


Fig. 2 – Al spectra in the full  $K$ -shell spectral window at different carbon layer thickness  $d_c$ .

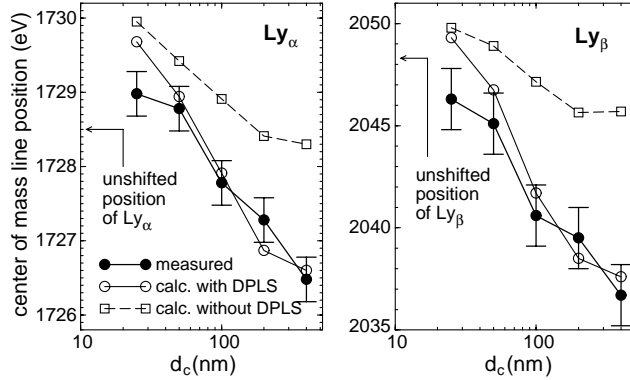


Fig. 3 – The center-of-mass line position (determined from the mean value of the frequencies at half-intensity on both sides of the peak of the line) of the  $Ly_\alpha$  and  $Ly_\beta$  line *vs.*  $d_c$ .

PET reflectivity. The spectra display the  $Ly_\alpha$  and  $He_\alpha$  lines together with their He- and Li-like satellites as well as the  $He_\beta$ ,  $He_\gamma$ , and  $Ly_\beta$  lines. Since these spectra were recorded without the Si  $K_\alpha$  reference line to avoid blending of the Si plasma lines (emerging at  $h\nu$  above the Si  $K_\alpha$ ) with the Al lines, the Al  $Ly_\alpha$  line was positioned at the same  $h\nu$  as in the spectra obtained with a superimposed Si  $K_\alpha$  reference line. Significant changes of the spectra with  $d_c$  are visible in fig. 2, particularly for the higher-energy lines ( $He_\beta$ ,  $He_\gamma$ ,  $Ly_\beta$ ), which show a clear increase in width (along with a decrease in intensity). These lines show also a considerable CM shift to lower energies with increasing  $d_c$ . For the  $Ly_\beta$  line, this trend is plotted in fig. 3. In addition to the line emission, the spectra exhibit a continuum with an exponential decay representing a temperature of 250 eV. It is attributed to free-bound emission from carbon and was also present in shots with targets without the Al SL. It characterizes the carbon temperature averaged over the total heated carbon depth (including the Sigradur substrate). It is of interest that in fig. 2 the ratios between the different line strengths (the line integrated over frequency) show no significant changes for different  $d_c$  indicating a rather constant temperature in the SL for the whole  $d_c$  range studied. *E.g.*, the  $Ly_\beta/He_\beta$  line strength ratio is  $0.4 \pm 0.02$ . Assuming LTE, this yields an effective temperature in the SL of  $480 \pm 20$  eV.

*Comparison with theory.* – We will now discuss the analysis of the spectra. First, the time history of the temperature and the density in the SL due to the hydrodynamic motion has to be calculated. In this context the electron energy transport is crucial. At the intensity of this experiment exceeding a few  $10^{17}$  W/cm<sup>2</sup>, it is no longer well described by Spitzer's heat conduction, because the mean free path of the energetic electrons generated at the critical density exceeds the depth of the heat wave propagating into the solid. As a consequence, calculations performed with the MULTI-fs code [16], which uses Spitzer's heat flow, failed to describe the measured constant temperature up to a depth of 400 nm in the solid. Thus, a kinetic model is needed. To avoid a sophisticated theory, we use here a simple model. We assume an energy deposition in the solid target which is caused by the hot electrons generated at the critical layer penetrating into the target. To account for the measured constant temperature in the target up to a depth of 400 nm, we apply a spatial deposition profile which is constant up to a depth given by the mean free path of the hot electrons, which is  $0.8 \mu\text{m}$  (in carbon) for the measured hot-electron temperature of 9 keV. The heating is assumed to occur only during the laser irradiation which is justified by the fact that the lifetime of the hot electrons in the solid is short ( $\approx 40$  fs) compared to the pulse duration of

the laser pulse. To simulate the measured spectra, one must further assume that the electrons propagate into the solid with an intensity of  $6 \times 10^{16}$  W/cm<sup>2</sup>. This means that about 50% of the absorbed laser intensity ( $\approx 1.2 \times 10^{17}$  W/cm<sup>2</sup>) is converted into energetic electrons propagating into the target. The resulting time histories (obtained with the one-dimensional MULTI hydro-code [17]) show an initial fast increase of the temperature in the SL up to about 800 eV during the heating phase of 300 fs and a subsequent expansion phase with decreasing temperature and density during a few ps. Gradients within the quasi-uniform SL are small (typically, relative temperature and density changes are less than 1% and 5%, respectively).

Next, from the time histories of electron temperature and density, the level populations have been calculated by the fully time-dependent CRAK (Collisional-Radiative Atomic Kinetics) code [18]. It determines the time histories of ground, non-autoionizing and autoionizing state populations in Al ions ranging from the Ne-like ground state to the fully stripped ion. Autoionizing levels are included in the model, since they are necessary for the consideration of satellite lines also observed in the experiments. In addition, they have an important effect on overall atomic kinetics since, at high electron densities, they can harbor significant population. Therefore, autoionizing and non-autoionizing energy level populations are calculated self-consistently in CRAK [18]. The CRAK code uses an extensive, atomic-physics database that was generated by the Los Alamos atomic structure and scattering codes CATS, ACE, and GIPPER [19]. Opacity effects on the atomic kinetics are small in the collision-dominated plasma considered here. They are taken into account by escape factors calculated for slab geometry and Stark broadened line profiles [20].

Finally, synthetic spectra were calculated by using CRAK-generated level populations and detailed line shapes. For the line shapes we include the effects of natural, thermal Doppler and Stark broadening due to the microfields of plasma ions and electrons. We consider ion Stark broadening within the scope of a static-ion approximation and the dynamic-electron broadening by a quantum relaxation theory [21, 22]. In addition, the DPLS effect is also included according to the theory of ref. [5] for all resonance and satellite lines. Furthermore, we take into account the Doppler shift due to the macroscopic motion of the SL, which is not negligible for SLs close to the target surface. Line broadening due to self-absorption is important for the strongest resonance lines and has been included by solving the radiation transport equation for the case of uniform slab of plasma [23]. Finally, the spectra were folded with the experimental resolution.

For comparing the calculated line emissions with the time-integrated measurements, the calculated spectra were time-integrated. We note that the typical calculated duration of the emission was around 1 ps. Although time-dependent measurements have not yet been performed with the layered targets used here, we can mention that we measured for the same irradiation conditions, but with massive Al targets, similar emission durations [24].

Figure 2 shows a comparison of the measured overview spectra with the calculation. To account for the carbon continuum, we added to the Al spectra a continuum  $\propto \exp[-h\nu/250 \text{ eV}]$ . The resulting calculated spectra show satisfactory agreement with the experiment. To reproduce the absolute values of the lines, we assumed in the calculation of the three spectra in fig. 2 an emitting surface with a diameter of  $6 \mu\text{m}$ . This is less than the measured X-ray spot size of  $13 \mu\text{m}$ , but still reasonable in view of the uncertainty in the measured absolute values. The agreement between calculation and measurement includes the increasing width and CM shift seen for the lines at higher energy ( $\text{He}_\beta$ ,  $\text{He}_\gamma$  and  $\text{Ly}_\beta$ ). It is noted that these lines are optically thin (mean optical depth  $\bar{\tau} < 0.1$ ), while for the more intense lines  $\text{Ly}_\alpha$  ( $\bar{\tau} = 0.87$ ) and  $\text{He}_\alpha$  ( $\bar{\tau} = 1.3$ ) opacity effects are important.

A comparison of calculated  $\text{Ly}_\alpha$  line shapes with the experiment is done in fig. 1. To demonstrate the effect of the DPLS, we plotted calculated spectra both with and without

DPLS. Clearly, at large depth ( $d_c = 400$  nm) the measured  $\text{Ly}_\alpha$  line as well as its He-like satellite is in better agreement with the calculation including DPLS. For the Al SL closest to the surface ( $d_c = 25$  nm), the line is slightly blue-shifted, which is caused by the motional Doppler effect. For the line profiles we observe the trend that the measured width is somewhat larger than the calculated width, in particular on the red wing. In principle, this can be related to the fact that in the experiment lateral gradients are present giving rise to emission from colder regions in the periphery of the spot not taken into account in our one-dimensional analysis. We emphasize that we systematically also produced good fits for the other lines ( $\text{He}_\alpha$ ,  $\text{He}_\beta$ , and  $\text{Ly}_\beta$ ) with their associated satellites when the DPLS was included in the calculation.

In fig. 3 we compare the measured and calculated CM shifts of the  $\text{Ly}_\alpha$  and the  $\text{Ly}_\beta$  lines as a function of the SL depth. For both lines, the measured CM shifts are in good agreement with the calculation, provided that DPLS is included. We note that we have positioned the Si  $K_\alpha$  reference line at  $h\nu = 1740.4$  eV, which is 0.5 eV larger than the value expected for cold Si [25]. This results from a best fit of the measured to the calculated  $\text{Ly}_\alpha$  CM shifts. Such a small shift may be possible if the  $\text{SiO}_2$  target is slightly heated by electrons or X-rays causing little ionization (the emission from  $\text{Si}^{1+}$  instead from  $\text{Si}^{0+}$  would result in a shift of 0.5 eV [26]). The knowledge of the exact absolute position of the Si  $K_\alpha$  line is of minor importance for the  $\text{Ly}_\beta$  line, for which the CM shifts are much larger than those for the  $\text{Ly}_\alpha$  line. It is of interest to mention that the  $\text{Ly}_\beta$  line calculated without DPLS shows after a blue-shift at small  $d_c$  (due to motional Doppler effect) also a small red-shift of  $\approx 2.6$  eV at  $d_c \geq 200$  nm, which is attributed to blending of the resonance line with satellites, but which is too small to explain the measured CM shift.

We calculated the typical electron density  $n_e$  and temperature  $T_e$  belonging to the different points in fig. 3 by time-averaging  $n_e$  with the  $\text{Ly}_\alpha$  or the  $\text{Ly}_\beta$  intensity as a weight. The resulting values for  $n_e$  increase from  $1 \times 10^{23}$   $\text{cm}^{-3}$  at  $d_c = 25$  nm to  $5 \times 10^{23}$   $\text{cm}^{-3}$  at  $d_c = 400$  nm, while the correspondingly averaged  $T_e$  values were 500 eV for all  $d_c$ , close to  $T_e$  determined from the  $\text{Ly}_\beta/\text{He}_\beta$  line ratio.

*Conclusions.* – In conclusion, we irradiated targets with 25 nm thin Al sample layers embedded in solid carbon with ultrashort laser pulses. The sample layer buried up to a depth of 400 nm was heated to effective temperatures of about 500 eV. The Al resonance lines show an increasing width and center-of-mass shift with increasing depth of the Al layer, which is attributed to an increasing density. The good agreement between measurement and calculation supports the recent dense-plasma line shift model of Junkel *et al.* [5]. Another interesting aspect of this experiment is the efficient electron transport into the solid target, which will be studied further in the future.

\* \* \*

This work was supported in part by the European Communities in the framework of the Euratom-IPP association, the SSP 1053 of the DFG, and the UCCSN.

## REFERENCES

- [1] GRIEM H. R., *Plasma Spectroscopy* (McGraw-Hill, New York) 1964.
- [2] WOOLSEY N. C. *et al.*, *J. Quantum Spectrosc. Radiat. Transfer*, **58** (1997) 975.
- [3] NGUYEN H. *et al.*, *Phys. Rev. A*, **33** (1986) 1279.
- [4] GRIEM H. R. *et al.*, *Phys. Rev. A*, **41** (1990) 5600.
- [5] JUNKEL G. C. *et al.*, *Phys. Rev. E*, **62** (2000) 5584.

- [6] LENG Y. *et al.*, *Phys. Rev. E*, **52** (1995) 4328.
- [7] RENNER O. *et al.*, *J. Quantum Spectrosc. Radiat. Transfer*, **58** (1997) 851.
- [8] WOOLSEY N. C. *et al.*, *J. Quantum Spectrosc. Radiat. Transfer*, **65** (2000) 573.
- [9] SAEMANN A. *et al.*, *Phys. Rev. Lett.*, **82** (1999) 4843.
- [10] GUETHLEIN G. *et al.*, *Phys. Rev. Lett.*, **77** (1996) 1055.
- [11] YOUNG B. K. F. *et al.*, *Phys. Rev. E*, **58** (1998) 4929.
- [12] FOURNIER K. B. *et al.*, *J. Quantum Spectrosc. Radiat. Transfer*, **71** (2001) 339.
- [13] KOCH J. A. *et al.*, *Phys. Rev. E*, **65** (2001) 016410-1.
- [14] EIDMANN K. *et al.*, *Europhys. Lett.*, **55** (2001) 334.
- [15] ANDIEL U., PhD Dissertation, Technische Universität München, 2001.
- [16] EIDMANN K. *et al.*, *Phys. Rev. E*, **62** (2000) 1202.
- [17] RAMIS R. *et al.*, *Comput. Phys. Commun.*, **49** (1988) 475.
- [18] HAKEL P., PhD Dissertation, Department of Physics, University of Nevada, Reno, 2001.
- [19] ABDALLAH J. jr. *et al.*, Los Alamos National Laboratory Report LA-11436-M, Vols. I and II, 1988.
- [20] MANCINI R. C. *et al.*, *J. Phys. B*, **20** (1987) 2975.
- [21] WOLTZ L. A. and HOOPER C. F. jr., *Phys. Rev. A*, **38** (1988) 4766.
- [22] MANCINI R. C. *et al.*, *Comput. Phys. Commun.*, **63** (1991) 314.
- [23] MIHALAS D., *Stellar Atmospheres* (Freeman & Co., San Francisco) 1978.
- [24] ANDIEL U. *et al.*, *Appl. Phys. Lett.*, **80** (2002) 198.
- [25] BEARDEN J. A., *Rev. Mod. Phys.*, **39** (1967) 78.
- [26] HOUSE L. L., *Astrophys. J., Suppl. Ser.*, **18** (1969) 21.